Evaluation of chemical stability of conducting ceramics to protect metallic lithium in Li/S batteries

Laurent Castro, Emmanuel Petit, Anass Benayad, Fabrice Mauvy, Brigitte Pecquenard, Frédéric Le Cras, Céline Barchasz

Evaluation of chemical stability of conducting ceramics to protect metallic lithium in Li/S batteries

L. Castroi[1], E. Petit[1], A. Benayad[2], F. Mauvy[1], B. Pecquenard[1], F. Le Cras[3], C. Barchasz[3]

[1] CNRS, Univ. Bordeaux, Bordeaux INP, ICMCB, UMR 5026, 33600 Pessac, France
[2] Univ. Grenoble Alpes, CEA, LITEN, DTNM, L2N, F-38054 Grenoble, France
[3] Univ. Grenoble Alpes, CEA, LITEN, DEHT, STB, F-38054 Grenoble, France

Abstract :

Among the different cutting-edge solutions currently under investigation, lithium metal technologies have received a renewed interest. Thorough research work is currently carried out to enhance the safety and cyclability of the lithium metal electrode, targeting high energy post-Li-ion systems such as the lithium/sulfur technology. This study aims at investigating different inorganic protective layers that could be placed at the surface of the lithium metal electrode in a lithium/sulfur system, in order to prevent the detrimental interactions with polysulfide species and electrolyte components. The chemical stability of the selected inorganic materials (amorphous thin films, crystalline ceramics and glass-ceramics) towards ether-based (polysulfides-containing) electrolytes was studied. Although being crucial for long term cycling of Li/S cells, this issue has not been addressed so far. The chemical composition and morphology of the different materials after immersion in different electrolytes were characterized by X-ray diffraction, XPS and SEM, and the most promising materials were evaluated in Li/S cells..

1. Introduction :

In the context of strengthening the global response to limit global warming, there is definitely a great challenge for improving energy storage systems [1,2], especially to fit electrified vehicles market. Since their commercialization in 1991 [3], the performances of Li-ion batteries have been steadily improved, especially in terms of lifetime and volumetric energy density [4,5]. This technology is now mature and their maximum energy densities are levelling off around 300 $Wh{\cdot}kg^{-1}$ [[2], [3], [4], [5], [6]]. As a consequence, there is a need for alternative electrochemical systems that could deliver higher gravimetric energy density at a lower cost, while maintaining a high cycle life and good safety properties. Among the different cutting-edge solutions currently under investigation, lithium metal technologies have received a renewed interest [[2], [3], [4], [5], [6], [7]]. The lithium metal (Li) used as negative electrode was discarded in the past after many safety events encountered during batteries operation [8]. Nowadays, metallic lithium is again on a good way to further increase the gravimetric energy density of Li-based electrochemical systems, due to its lightweight and a low operating voltage [7]. Therefore, it is more necessary than ever to enhance the stability of the Li metal electrode upon cycling, especially when used in the high energy lithium/sulfur or lithium/oxygen post-Li-ion systems [6].

Lithium/sulfur batteries (Li/S) have been under intense studies for the last two decades, with a particular interest since 2010 [9,10]. The use of elemental sulfur as an active material allows for high theoretical specific capacity (1675 $mAh{\cdot}g_S^{-1}$) at about 2.1 V versus Li^+/Li, while sulfur has also the benefit of being abundant, cheap and non-toxic as compared to conventional transition metal oxides [11]. While over the last decade main efforts were mostly dedicated to the sulfur positive electrode, more recent studies were focused on a better understanding and improvement of metallic lithium/liquid electrolyte interface by developing alternative electrolyte formulations [[12], [13], [14]]. Ether solvents are usually selected for Li/S system, in place of carbonate solvents commonly used in Li-ion cells, due to their stability against polysulfides [15,16]. Nevertheless, it was demonstrated that ether solvents decompose on the lithium electrode, forming lithium alkoxy species [[17], [18], [19], [20]], which do not allow for an efficient lithium metal passivation and finally result in a rough morphology and a poor lithium cycling efficiency [17]. Recently, the effect of electrolyte additives such as FEC or $LiNO_3$ was investigated to improve the passivation of the lithium electrode in liquid electrolytes [[21], [22], [23], [24], [25]]. Both additives have shown a beneficial effect against lithium polysulfides shuttling, which depends on their concentration, improving the cycle life and the coulombic efficiency, this latter remaining limited anyway [26].

The formation of massive SEI on the lithium electrode was reported in ether-based liquid electrolytes, especially when using high areal capacity sulfur electrodes (>4 $mAh{\cdot}cm^2$) [9,27,28]. At the same time, when the electrolyte contains SEI forming additives and/or dissolved polysulfide species, a progressive consumption of lithium and electrolyte upon SEI formation occurs that ends up with the cell sudden death due to electrolyte and/or active lithium shortage [9,27]. As a consequence, prolonged cycling of

highly loaded sulfur electrodes in a liquid electrolyte is still an issue, and hindrance of this domino effect is particularly critical for the development of Li/S technology. Cycle life of the metallic lithium has to be extended through electrolyte formulation [29], or more preferably by preventing the latter from any contact with the organic electrolyte [[30], [31], [32]]. Besides, the developments should usefully tackle the issue of lithium dendritic growth, which is still a concern for the safety of the final application. So far, only few studies were focused on lithium protection, for example using Li_3N protective layer or a film made of close-packed carbon nanospheres [30,33]. Polymer coatings and inorganic protective solutions [[34], [35], [36]] have attracted much more interest, with promising results shown in terms of lithium cycling efficiency. Glassy LiPON and Li_3PO_4 thin films have also been applied in order to mitigate dendrites formation, enhance cycle life and increase lithium cycling efficiency [[37], [38], [39]].

In this paper, we aimed at investigating different inorganic protective layers that could protect the lithium metal electrode in a Li/S system, in order to prevent the detrimental interactions with polysulfide species and electrolyte components, and then to possibly hinder the morphological evolution of the metallic anode. For this purpose, different candidates were selected and compared: lithium phosphate amorphous thin films, Nasicon-type $Li_{1.5}Al_{0.5}Ge_{1.5}(PO_4)$ or LAGP, $Li_{1+x+y}Al_xTi_{2-x}Si_yP_{3-y}O_{12}$ or LICGC®. LiPON is a widely used thin film electrolyte in all-solid-state thin-film batteries using metallic lithium as a negative electrode [42]. Its deposition by reactive sputtering of a Li_3PO_4 target in a nitrogen plasma leads to dense thin films (about 1 µm) with good conductivity (in the order of 10^{-6} S·cm^{-1}), and can be carried out at the industrial scale [41,43]. LAGP was considered due to its high ionic conductivity (compared to LiPON, in the order of 10^{-4} S·cm^{-1}) and its ability to be prepared in the shape of dense pellets. Finally, LICGC® glass-ceramics membranes were also purchased as a commercial product from Ohara company [44], providing a good alternative material being dense and high ionically conductive. The chemical stability of these inorganic coatings towards ether-based polysulfides-containing electrolytes was studied by comparison of the properties (structure, composition, morphology, ionic conductivity) of pristine materials and the ones after a prolonged contact with the electrolyte components. Although being crucial for long term cycling of Li/S cells, this issue has not been addressed so far. The most promising materials were then selected in order to be evaluated as a lithium metal protective layer in full Li/S cells.

2. Experimental procedure

2.1. Synthesis of inorganic materials

The preparation of Li_3PO_4 and LiPON thin films was achieved by radio-frequency magnetron sputtering of a Li_3PO_4 target under a pure argon (Li_3PO_4) or nitrogen (LiPON) atmosphere in a Plassys chamber directly connected to an argon-filled glove box at a power density of 2 W·cm^{-2}, a total pressure of 1 Pa and a gas flow of 40 ml·min^{-1}. The deposition was performed without any intentional heating of the substrate. Three different substrates were used for different purposes: 1) silicon wafer covered by barrier layers (SiO_2, Si_3N_4) was used for the characterization of the thin film layers, 2) glass plate with a stainless steel electrode was used for ionic conductivity measurements and 3) a disk of Li foil was used to carry out the electrochemical characterizations. For this last substrate, and due to the reactivity of Li with nitrogen, a thin layer of Li_3PO_4 (100 nm) was first deposited on Li followed by a thicker layer of LiPON (typically ~1 µm). The chemical composition of thin films is given in the Table S1.

The synthesis of $Li_{1,5}Al_{0,5}Ge(PO_4)_3$ (LAGP) was carried out using a sol-gel process [40] that allows an efficient control of the particles size and Li release and leads to reproducible ionic conductivity measurements. Germanium and aluminum alkoxides ($Ge(OC_2H_3)_4$, Aldrich 99.95% pure and $Al(OC_4H_9)_3$, Aldrich technical grade), lithium and ammonium salts ($CH_3COOLi{\cdot}2H_2O$, Aldrich reagent grade and $(NH_4)_2HPO_4$, Aldrich > 98%) were used as reactants. The stoichiometric mixture of alkoxides was dissolved in butanol and maintained at 70 °C before the solution of salts (ammonium phosphate and Li acetate dissolved into water) was added. This led to the instantaneous formation of a white gel. Sustained mechanical stirring was carried out during 2 h at 70 °C. Then, freeze-drying was used both to remove the solvents and to avoid agglomeration of particles. After this step, different annealing conditions (temperature ranging from 750 to 850 °C and duration between 5 h and 20 h) were used to evaluate their influence on the purity and the crystallinity of the LAGP material. Whatever the conditions, some impurities (mainly $AlPO_4$) were always present on the XRD diagram (Fig. S1). A thermal treatment at 800 °C during 10 h in a gold crucible was found to be a good trade-off between a good crystallinity, a small amount of impurities, and limited Li release. Then the powder was ground during 5 h using a planetary ball mill (Fritsch) with agate balls and bowl. The average grain size, measured by laser diffraction, was in the order of 400–500 nm. Cylindrical pellets (8 mm diameter) of LAGP were prepared by spark plasma sintering (SPS) using the following conditions: a constant pressure of 75 MPa is applied, then a 100 °C·min^{-1} heating rate until 500 °C and a 50 °C·min^{-1} heating rate from 500 to 700 °C, maintained for duration of 2 min. The pellets were then polished and their compactness of 90 ± 1% was measured by pycnometry in isopropanol. LICGC® ($Li_{1+x+y}Al_xTi_{2-x}Si_yP_{3-y}O_{12}$) glass-ceramics membrane was purchased from Ohara Company (1 inch square, 0.15 mm thick).

2.2. Charaterization techniques

The thickness of thin films was determined using a Tencor profilometer alpha step 200. The P, N and O contents were determined on thin films deposited on Si substrate by electron microprobe analysis (EPMA, Cameca SX100) using InP, Si_3N_4, $Y_3Fe_5O_{12}$ and Si (for substrate) as calibration standards. The Li and P contents were measured using an inductively coupled plasma–optical emission spectrometer (ICP–OES) (Varian 720ES) by dissolving beforehand thin films deposited on the glass substrate in 10 ml of HCl. The wavelengths of the emission line were 460.289 nm for Li and 214.914 nm for P. The measurement uncertainty of ICP was around 2%.

The surface morphology of thin films and ceramics was investigated by scanning electron microscopy using a Jeol 6700-F microscope. To avoid a possible charging effect induced by the electron beam on the samples, the films were systematically coated with a thin gold film before observations. The homogeneity of LiPON thin film composition was checked by Auger spectroscopy depth profiling (VG MICROLAB 310F apparatus). The structure of ceramics was studied by X-ray diffraction (XRD) using a PANalytical X'Pert with CuKα radiation (λ = 1.5418 Å).

Table 1
Main properties of selected ionic conductors.

Type	NASICON		Glassy thin-films	
Material	LAGP $Li_{1.5}Al_{0.5}Ge_{1.5}(PO_4)_3$	LICGC® $Li_{1+x+y}Al_xTi_{2-x}Si_yP_{3-y}O_{12}$	LiPON	Li_3PO_4
σ_{tot} (S·cm^{-1}) at RT	10^{-4}	10^{-4}	$2.5 \cdot 10^{-6}$	$8.4 \cdot 10^{-7}$
Stability towards Li	No	No	Yes	Yes
Densification and Li departure	Good densification and no departure of Li (sol-gel), Ge^{4+} reduction	Commercial product, Ti^{4+} reduction	Good densification	Good densification, no Li departure
Accessible thickness and surface resistance	~100 µm 100 Ω·cm^2	~100 µm 100 Ω·cm^2	~1 µm ~33 Ω·cm^2	~1 µm ~125 Ω·cm^2

The ionic conductivity measurements were achieved using symmetrical cells by Electrochemical Impedance Spectroscopy (EIS) using a Solartron 1260 analyzer. Ceramic pellets (8 mm diameter), shaped and sintered by SPS, were covered by a thin film of gold. Measurements on thin films were achieved on the stainless steel/LiPON (or Li_3PO_4/stainless steel) stacks, with a design providing four separated measurement points as described elsewhere [41]. The gold and stainless steel electrodes were deposited by radio-frequency magnetron from the corresponding target in an Ar atmosphere. The impedance measurements were carried out in a frequency range from 1 Hz to 1 MHz, with a 50 mV AC voltage amplitude and with a 5 °C increment from 25 °C to 95 °C. Impedance spectra fitting was carried out using ZView 2 commercial software. The measurement uncertainty of ionic conductivity was around 10% at maximum (possible error on the determination of exact surface and thickness).

X-ray photoelectron spectroscopy (XPS) analysis was performed to study the change in the surface chemical composition of the inorganic layers prior and after contact with the different electrolyte components. Measurements were done using Versaprobe II PHI 5000 (ULVAC-PHI) spectrometer using a 100 µm focused monochromatic Al-Kα X-ray source (1486.6 eV) beam. Survey spectra were performed over a spectral range of 0–1200 eV to identify the elements present in the materials within the pass energy of 117 eV, corresponding to an energy resolution of 1.6 eV and an acquisition time of 0.5 s·eV^{-1}. The high-resolution spectral analysis was performed using a pass energy of 23 eV allowing an energy resolution of 0.5 eV. All spectra were recorded using dual beam charge neutralization to reduce the differential charging effect. The spectra did not show any modification (peak shift or shape change) under beam exposure. The binding energy peak calibration was performed using the C1s core level of contamination carbon as well as alkyl carbon, systematically present at the surface of the samples, at 285 eV. All materials, pristine and after prolonged contact with the electrolyte components, were transferred to the XPS spectrometer using a transfer capsule to avoid air contamination.

2.3. Chemical stability tests

A conventional liquid electrolyte composition, i.e. 1 M lithium bis(trifluoromethane sulfonyl)imide salt (LiTFSI, 99.95%, Solvay) in a mixture of tetraethylene glycol dimethyl ether (TEGDME, 99%, Aldrich, stored on molecular sieves) and 1,3-dioxolane (DIOX, anhydrous, 99.8%, Aldrich, stored on molecular sieves) in 1/1 volume ratio, was selected for chemical stability tests. Chemical stability tests were also achieved using a catholyte solution, composed of dissolved lithium polysulfides in the same electrolyte mixture (LiTFSI 1 M + TEGDME/DIOX 1/1). These polysulfides were chemically synthetized in an argon-filled glovebox, in the electrolyte solvents directly with the equivalent composition Li_2S_6 0.25 M. This composition was selected as being representative of a polysulfides concentration in a Li/S battery, taking into account a reasonable electrolyte/sulfur ratio (E/S ~ 20) with a reasonable viscosity. Thin films of Li_3PO_4 and LiPON deposited on silicon wafers (1 µm thick, 4 mm × 5 mm), piece of LICGC® (5 mm × 5 mm) and ceramics LAGP powders (0.7 g) were then immersed into each type of solution (approximately 4 g of electrolyte) during 2 weeks inside a glove box. Then, the electrolyte (or catholyte) was removed and samples were rinsed three times with anhydrous DIOX. The evolution of the properties of materials (structure, morphology, ionic conductivity) was assessed after prolonged contact of these materials with the electrolyte components.

2.4. Electrochemical characterization

As purchased sulfur (−100 mesh, Refined, Aldrich) was used as an active material, mixed with carbon black (SuperP Li®, Imerys) and carbon fibers (VGCF®, Showa Denko) conductive additives, and with CMC/SBR polymer binders in water (carboxymethylcellulose as a dispersing agent, and styrene-butadiene rubber as a binder). Electrode composition was fixed to 75/10/5/10 wt% (S/SP/VGCF/binder). After high speed dispersion, the ink was casted onto a 20 µm thick aluminum current collector using a doctor-blade coater (5 $mg_S \cdot cm^{-2}$). Electrodes were then dried at 55 °C during 24 h, cut into Ø 14 mm disks (surface area of 1.539 cm^2), exposed to additional drying at RT under vacuum and finally introduced in an argon-filled glove box for coin cells assembly. Commercial battery grade lithium foil (Albemarle, 135 µm thick) was used as negative electrode.

CR2032 two-electrode Li/S coin cells were assembled in an argon-filled glove box, using the standard liquid electrolyte composition: LiTFSI 1 M + TEGDME/DIOX 1/1. Coin cells were prepared by stacking positive electrode disk (Ø 14 mm), a layer of thick polyolefin non-woven fabric serving as an electrolyte reservoir (Ø 16.5 mm, Viledon®, Freudenberg), a polypropylene microporous separator (Ø 16.5 mm, Celgard®2400), a disk of lithium metal (Ø 16 mm, treated or not protected) and a stainless steel spacer (Ø 16 mm). 150 µl of liquid electrolyte were poured onto the separators and the excess of electrolyte was drained out while crimping the coin cell. Coin cells were cycled at constant current in the voltage range [1.5–3.0] V vs Li^+/Li on Arbin® battery tester, at 20 °C and at varying C-rates. Cell capacities and current densities were calculated considering the theoretical specific capacity of sulfur (1675 $mAh \cdot g^{-1}$). Post mortem observations were carried out in an argon-filled glove box, after prolonged cycling and cell disassembly.

3. Results and discussion

3.1. Compatibility study between inorganic coationgs and electrolyte components

Some inorganic Li ionic conductors were selected (Table 1), including inorganic amorphous thin films (Li_3PO_4, LiPON), crystalline ceramics (Nasicon-type $Li_{1.5}Al_{0.5}Ge_{1.5}(PO_4)$ or LAGP) and glass-ceramics ($Li_{1+x+y}Al_xTi_{2-x}Si_yP_{3-y}O_{12}$ or LICGC®). While LiPON and Li_3PO_4 thin film electrolytes are used in lithium metal all-solid-state thin-film batteries, LAGP was considered due to its higher ionic conductivity and LICGC® glass-ceramics membranes as a commercial product. In the view to implement these materials into Li/S cells, the stability of thin films as well as bulk ceramic materials (LAGP powder and LICGC® commercial membrane) was evaluated when immersed in electrolyte component, either composed of lithium salt (LiTFSI) dissolved in a mixture of ether solvents (TEGDME/diox 1/1 vol., so-called Ele. samples), or polysulfides-containing (0.25 M Li_2S_6) electrolyte (so-called PS samples).

3.2 Evolution of composition (bulk, surface), structure and morphology

The chemical composition, structure and morphology of the different materials after immersion in the two types of electrolytes were characterized by ICP-OES, EMPA, X-ray diffraction as well as XPS and SEM. Change of the LiPON morphology was observed after immersion of the thin film in the polysulfide-containing electrolyte (Fig. 1). No degradation or change of the chemical composition of the LiPON layer was measured by combined ICP /EPMA measurements. Since no change in the characteristic peaks of LiPON (P2p, O1s, N1s) was observed as well, the change of the surface morphology after immersion might be attributed to salt decomposition (LiF) and/or microstructure coarsening (local evolution of sub-oxides and sub-nitrides). More specifically, no trace of sulfur was detected in the material after two weeks of immersion. Similar results were obtained for Li_3PO_4 thin film.

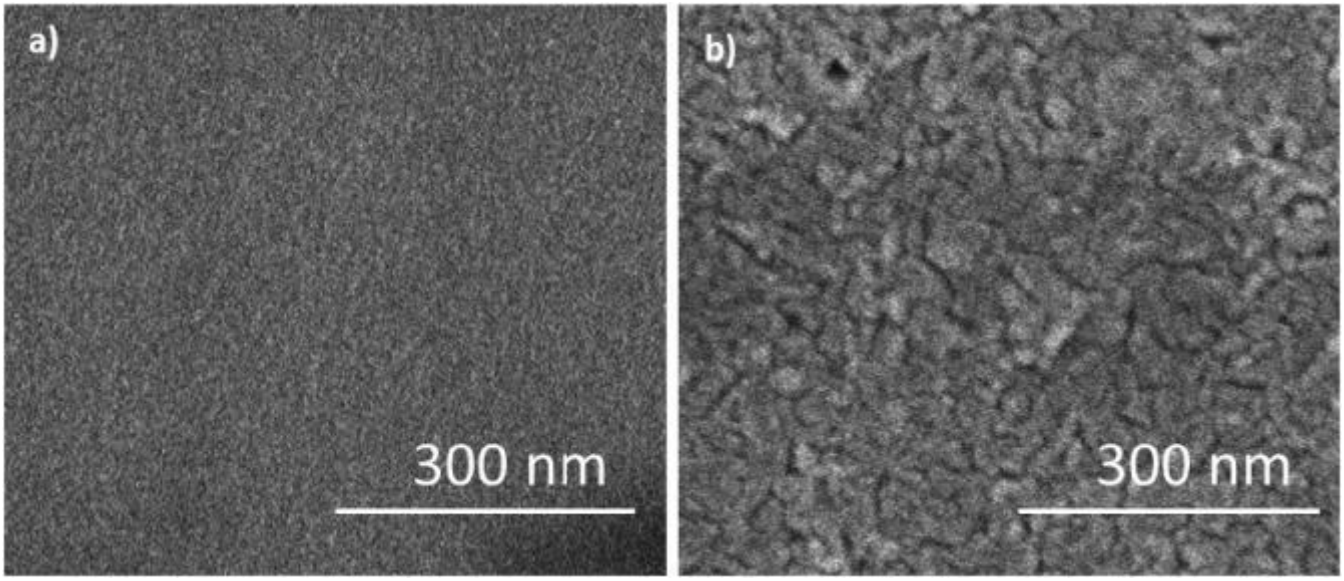

Fig. 1. SEM picture of a LiPON thin film layer before (a) and after (b) immersion in a polysulfides-containing electrolyte.

After two weeks of immersion in the electrolyte, the structure of Nasicon-type LAGP was preserved as evidenced in Fig. 2, while the morphology of LAGP particles was slightly modified only. Similar observations were made on LICGC® films (Fig. S2). The initial morphology of the commercial film shows the presence of cracks, which is in agreement with literature data [45], while the surface seems to be much smoother after immersion in the polysulfides-containing electrolyte. As for LiPON film, the change of the surface morphology is mostly attributed to the extreme surface that does not affect the bulk properties of the material, as evidenced by XRD data.

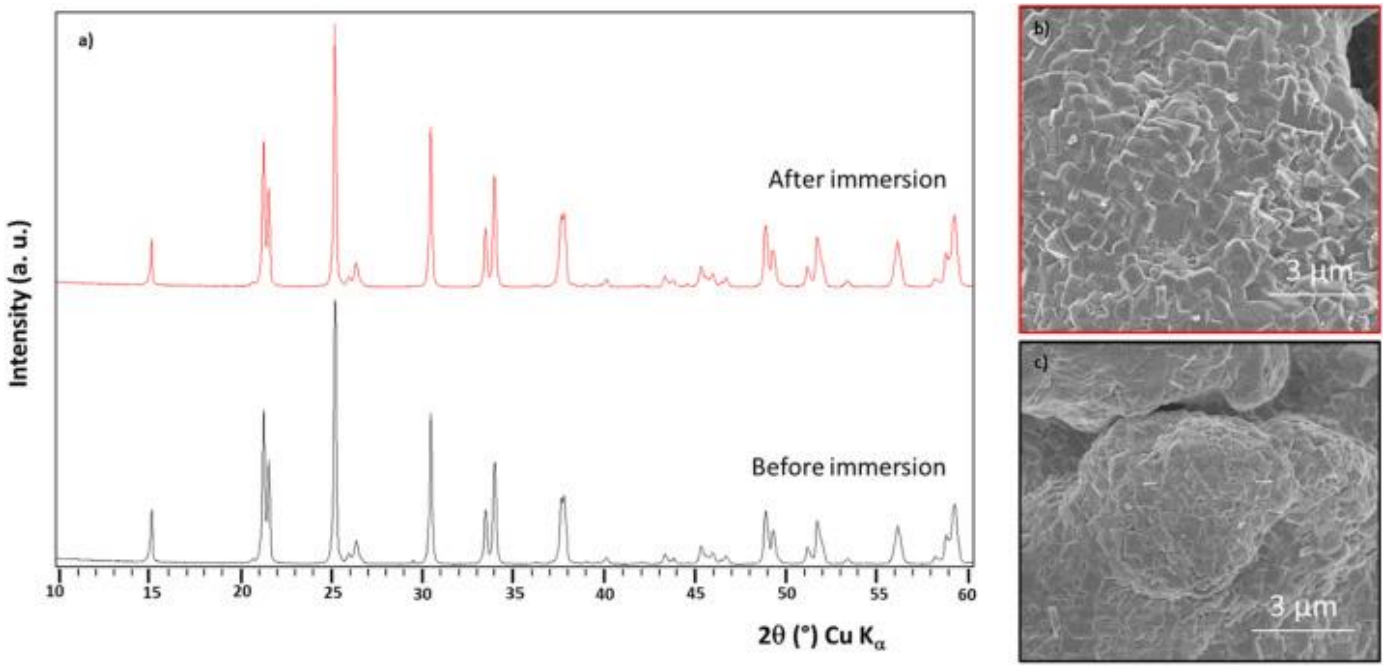

Fig. 2. Left: XRD pattern (a) of LAGP material before (black) and after (red) immersion in a polysulfides-containing electrolyte. Right: SEM picture of LAGP powder recorded after (b) and before (c) immersion in a polysulfides-containing electrolyte. (For interpretation of the references to color in this figure legend, the reader is referred to the web version of this article.)

The surface composition of the same materials was probed before and after immersion in different electrolyte solutions by XPS in order to highlight possible modifications of the chemical composition at the surface. In the case of Li_3PO_4, the XPS analyses performed before and after immersion in LiTFSI salt mixed with ethers (Ele) or polysulfides (PS)-containing electrolytes, labeled Li_3PO_4-Ele and Li_3PO_4-PS, are reported in Fig. S3. Regarding the surface composition of Li_3PO_4 film, no significant structural change

was evidenced. The PO_4 poly-anion remains almost unchanged after immersion in electrolytic solutions. The P 2p peak is fitted using one doublet $2p_{3/2}$ and $2p_{1/2}$, associated to spin-orbit coupling, corresponding to phosphorus in $(PO_4)^{3-}$ environment. The O 1s core level recorded before immersion is the signature of O^{2-} ions in Li_3PO_4, as well as sub-oxides at higher binding energies which are assigned to oxygen defects (–OH and carbon oxide groups) at the extreme surface. The C 1s peak shows the presence of contamination carbon and surface carbon oxide groups. The intensity of this peak decreases after immersion in the electrolyte solution. The F 1s and S 2p core levels recorded after immersion show the formation of LiF and poly-oxysulfides, resulting from LiTFSI decomposition. The deposition of Li_2S was also noticed in the case of Li_3PO_4 in ether-based electrolyte. The immersion into polysulfides-containing electrolyte does not drastically modify the surface contamination of Li_3PO_4, in particular in terms of sulfur species, and the PO_4 signature is still clearly visible at the surface.

In the case of the surface composition of LiPON film (Fig. 3), no significant structural change was evidenced neither. As for Li_3PO_4, the PO_4 poly-anion remains almost unchanged after immersion in the electrolytic solutions. The O 1s core level registered before immersion is the signature of O^{2-} ions and sub-oxides in Li_3PO_4. Looking at N 1s spectra, the signature of divalent and trivalent nitrogen atoms is observed. More precisely, the presence of NO_2 species associated to surface degradation process of trivalent nitrogen on the surface is noticed in the N 1s peak after immersion in the two electrolytes [46]. As for Li_3PO_4, the F 1s and S 2p core levels recorded after immersion in the polysulfides-free electrolyte show the formation of LiF and poly-oxysulfides already, resulting from LiTFSI decomposition. In this case, there is no evidence of Li_2S at the surface of LiPON thin film after immersion in both electrolytes.

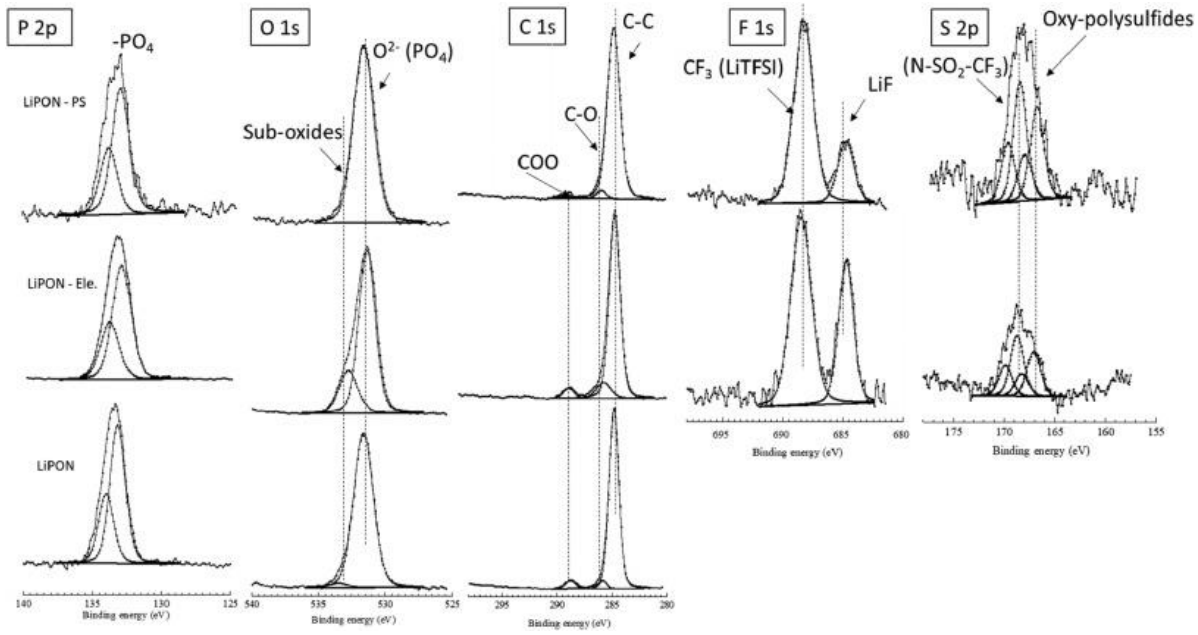

Fig. 3. P 2p, O 1s, N 1s, F 1s and S 2p core levels recorded at the surface of LiPON thin film before and after immersion in ethers (Ele.) and polysulfides (PS)-containing electrolytes.

Similarly, LAGP powder was immersed in the different electrolytic solutions, and the surface composition of the Nasicon-type structure does not seem to change after immersion (Fig. 4). In particular, signals of germanium, aluminum and phosphorus atoms remain unchanged, with Ge^{2+}, Al^{3+} and P^{5+} (like in PO_4) valence states. Surprisingly, in the case of polysulfides-containing electrolyte, deposition of LiTFSI salt at the surface was observed, without significant decomposition of electrolyte components, while deposition of LiF and organic species was observed already in the case of LAGP powder immersed in the polysulfides-free electrolyte [47]. Similar results were observed for LICGC® membrane when immersed in polysulfides-containing electrolyte (Fig. S4).

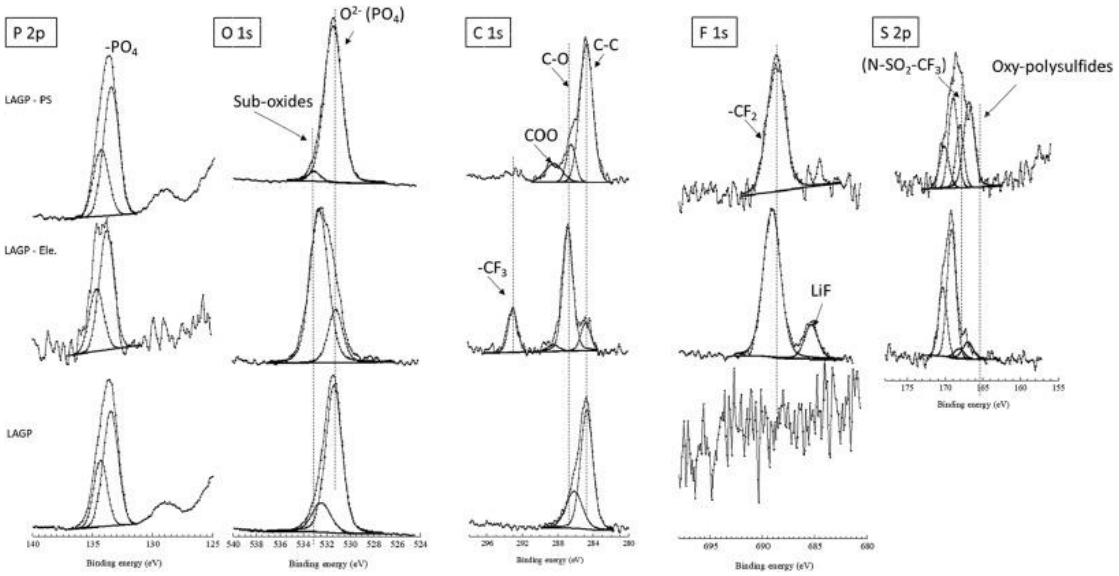

Fig. 4. P 2p, O 1s, C 1s, F 1s and S 2p core levels recorded at the surface of LAGP powder before and after immersion in ethers (Ele.) and polysulfides (PS)-containing electrolytes.

To conclude from XRD, SEM and XPS analyses, some degradation products were detected at the materials surface after contact with the polysulfides-free electrolyte already, such as the formation of LiF and poly-oxysulfides, which was attributed to decomposition products of LiTFSI. However, the bulk properties of all materials immersed in the two electrolytes were not significantly affected.

3.3 Evolution of ionic conductivity measurements

The ionic conductivity of the pristine materials was measured at first. Typical examples of Nyquist impedance plots are reported in Figs. 5 and S5. The ionic conductivities measured for Li_3PO_4 and LiPON were respectively $8.4 \cdot 10^{-7}$ S·cm^{-1} and $2.5 \cdot 10^{-6}$ S·cm^{-1} at 25 °C, with an activation energy around 0.56 eV for LiPON (around 0.67 eV resp. for Li_3PO_4), in good accordance with literature values [41]. The ones of LAGP and LICGC® membranes were respectively measured to about $2 \cdot 10^{-4}$ S·cm^{-1} and 10^{-4} S·cm^{-1} at 25 °C, and an activation energy was determined around 0.37 eV.

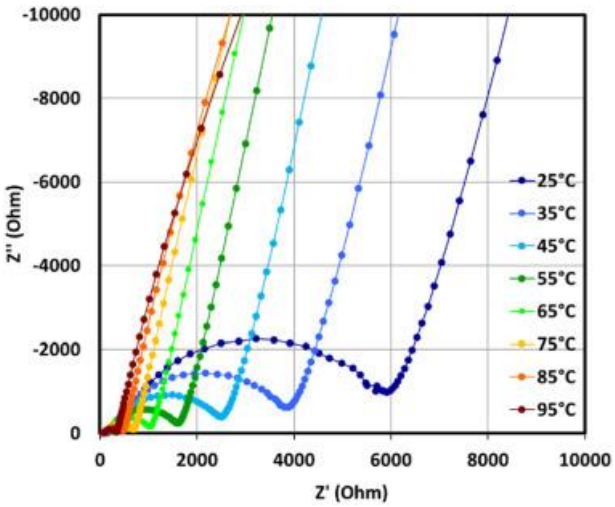

Fig. 5. Nyquist plot recorded for pristine LAGP pellet over the temperature range.

The ionic conductivity properties of the materials were also measured following immersion in the two electrolytes for two weeks. Fig. 6 shows that immersion into polysulfide-containing electrolyte did not significantly modify the ionic resistance of the material. Only a slight evolution of the spectrum is visible, mainly at low frequencies, that is likely ascribed to an increase of surface roughness of the film (Fig. 1).

The physico-chemical (XPS, XRD and SEM) and electrochemical (EIS) characterizations are of importance, showing that all the protective solutions that have been evaluated in this work are stable enough against Li/S electrolyte components. In turn, these materials could be applied to lithium as protective solutions against dendrites and polysulfides diffusion. LAGP and LICGC® materials being unstable towards lithium, Li_3PO_4 and LiPON thin films were evaluated first in Li/S coin cells.

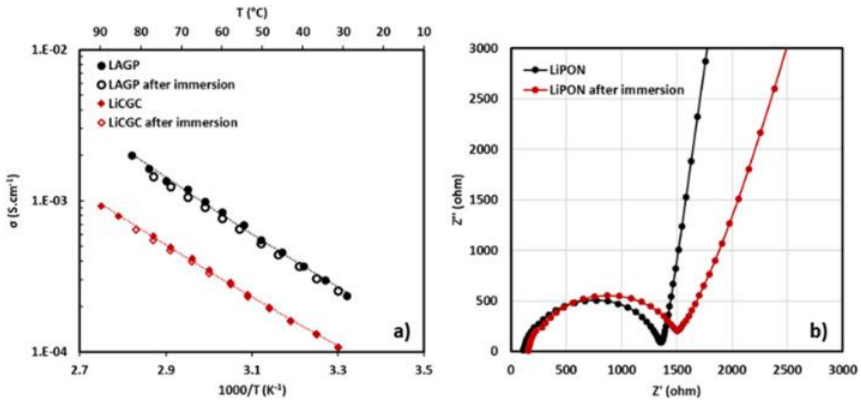

Fig. 6. a) Arrhenius plot obtained for LICGC® (red) and LAGP (black) membranes before (full markers) and after (empty markers) immersion into a polysulfides-containing electrolyte. Linear fits are presented with dotted lines (red and black). b) Nyquist plots obtained at room temperature for LiPON thin films before (black) and after (red) immersion into a polysulfides-containing electrolyte. (For interpretation of the references to color in this figure legend, the reader is referred to the web version of this article.)

3.4 Characterization of coated lithium electrodes

As previously mentioned, due to the reactivity of metallic lithium with nitrogen, a thin Li_3PO_4 film (~100 nm) was first deposited on lithium, before proceeding in depositing a thick layer of LiPON (typically around 1 µm), using RF magnetron sputtering. A good adhesion of thin films was observed on the negative electrode and the Li_3PO_4 thin film was efficient enough to protect the lithium electrode against the formation of Li_3N (Fig. 7a) to c). Grey bright surface of metallic lithium was preserved, while the electrode surface was as smooth as observed for pristine lithium foil. Auger analyses revealed a clean and well-defined interface between lithium and LiPON layers, and a limited amount of contaminants (Li_2CO_3, Li_3N) (Fig. 7d). The quantification of oxidized lithium by Auger spectroscopy and the limited accuracy of the method is rather difficult, but the fact remains that the N/P and O/P ratios can be determined close to 1 and 3 respectively.

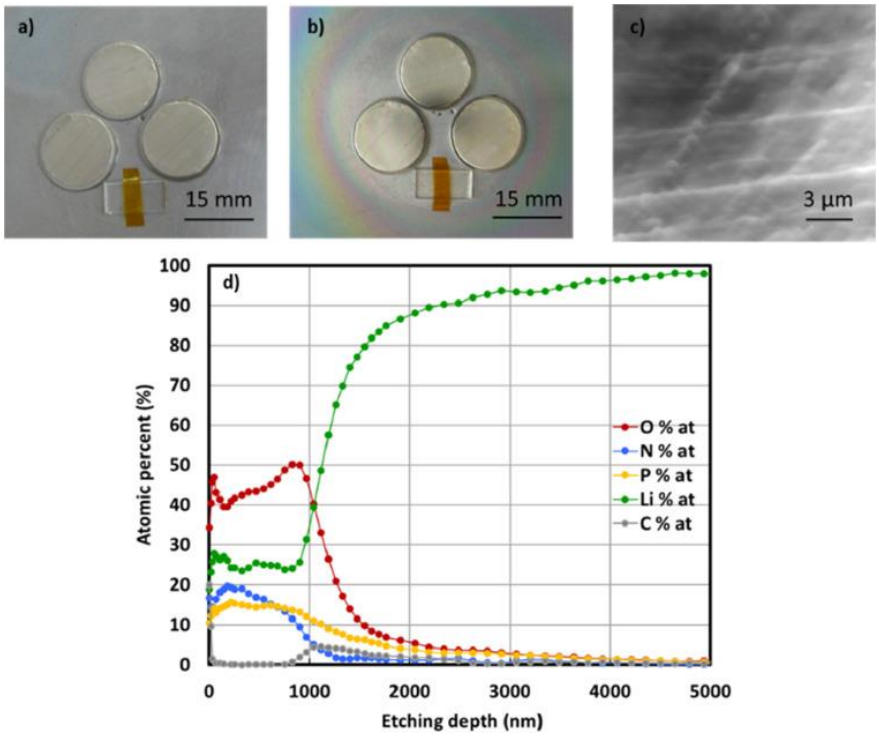

Fig. 7. Top: lithium metal electrodes (Ø16 mm) before (a) and after (b) LiPON deposition by radio-frequency magnetron sputtering. c) Image of the LiPON-coated lithium electrode surface observed in the Auger spectrometer. Bottom (d): Auger profile of a lithium metal electrode coated with Li_3PO_4/LiPON thin film (100 nm/1 µm).

The protected lithium metal electrodes were then characterized in Li/S coin cells at different C-rates using a thick sulfur electrode (5 $mg_S \cdot cm^{-2}$) and a standard electrolyte composition [15]. Low C/100 rate was first applied to coin cells and compared to a non-protected lithium metal anode, to evaluate the efficiency of thin film coatings towards polysulfides shuttle mechanism. Indeed,

at low C-rate, polysulfide species have enough time to shuttle between the two electrodes, except in the case of an efficient protective solution in the battery [48]. Fig. 8 compares the charge/discharge profiles that are obtained with a bare lithium metal anode (a) and a LiPON-protected lithium electrode (b). The shuttle mechanism, occurring at about 2.45 V during charge, is indeed significantly reduced by the presence of LiPON coating, even if the latter is not fully suppressed. It is also worth to mention that the cell with un-protected lithium could not be cycled at C/100 due to severe shuttle mechanism resulting in an infinite charge, while LiPON and Li_3PO_4 coated lithium electrodes could be cycled for more than 100 cycles.

LiPON and Li_3PO_4 coatings were then evaluated at a higher C/20 rate, and compared with a reference cell comprising a non-protected lithium electrode (Fig. 8c). Similar electrochemical properties were obtained for reference and lithium protected Li/S cells, in terms of capacity retention and coulombic efficiency. Unfortunately, despite the presence of a thin film coating at the lithium metal interface, post mortem observations after cycling and cell disassembly allowed to evidence a marked degradation of the lithium metal electrode. Indeed, as clearly visible in (Fig. 8c) insert, lithium surface is fully covered with a mixture of lithium foam and polysulfides after cycling, which shows the limited effect of thin film coating on the lithium metal protection. Li/S technology being intended for high energy systems, a high sulfur loading above 5 $mg_S \cdot cm^{-2}$ in the positive electrode is a target for the final application. With such a loading, the thickness of lithium electrode which is stripped and plated at each cycle is significant (12 to 30 µm in average), especially when compared with the 1 µm thick thin film coating. In turn, thin films may not be mechanically resistant enough, and break upon repetitive cycles of charge/discharge, leading to exposure of lithium metal surface to polysulfides and electrolyte components and the formation of solid electrolyte interphase products.

As a perspective, to overcome the low mechanical properties of thin films and electrochemical stability issues of the bulk ceramics, multilayer ceramic electrolyte membranes need to be envisaged. Investigating additional interlayers such as polymer and organic coatings may also be a relevant strategy to compensate the fragile behavior of inorganic protective layers.

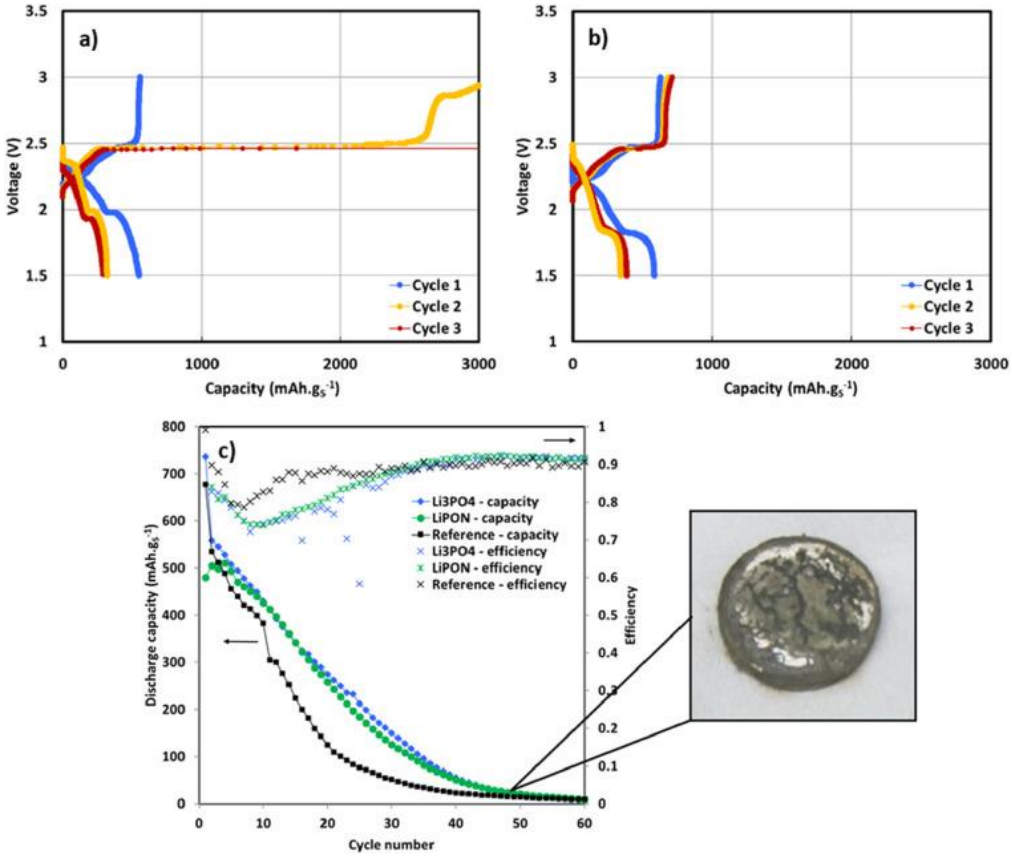

Fig. 8. Top: Initial charge/discharge profiles of a Li/S cell cycled at C/100 using a non-protected lithium metal electrode (a) and a LiPON-protected lithium metal electrode (b). Bottom (c): Electrochemical performances at C/20 of Li/S coin cells using lithium metal protected electrodes (LiPON or Li_3PO_4) or non-protected reference lithium (black). Onset: photography of a protected lithium metal electrode after prolonged cycling, evidencing the massive SEI formation.

4. Conclusion

In this paper, different inorganic protective layers were investigated, ranging from amorphous thin films (Li_3PO_4, LiPON) to crystalline ceramics or glass-ceramics (LAGP and LICGC®). The materials properties (structure, composition, morphology, ionic conductivity) were characterized, as well as their chemical stability towards electrolyte components. The stability of thin films and ceramic materials was evaluated when immersed in a polysulfides-containing electrolyte. The chemical composition and morphology of the different materials after immersion were characterized by Auger spectroscopy depth profiling, X-ray diffraction, XPS and SEM, and the results were compared with the ones obtained for a polysulfides-free electrolyte. No severe degradation of the materials was observed in this study, in particular regarding the bulk properties (ionic conductivity). Some degradation products were detected at the materials surface after contact with the polysulfides-free electrolyte already, which were attributed to LiTFSI decomposition. The most promising materials (Li_3PO_4 and LiPON) were selected and processed as thin films and evaluated in Li/S cells. Unfortunately, under dynamic conditions (galvanostatic cycling with highly loaded sulfur electrodes); Li_3PO_4 and LiPON thin films were not mechanically stable enough to follow lithium stripping/plating cycles, and a strong degradation of the lithium metal electrode surface was clearly observed. In turn, thin film coatings (1 µm thick only) may not be mechanically resistant enough, and break upon repetitive cycles of charge/discharge of the lithium electrode, leading to lithium metal surface exposed to polysulfides/electrolyte components and SEI formation. As a perspective, multilayer coating systems may be envisaged in the future, as an efficient solution to provide lithium with a mechanically resistant and chemically stable protective membrane. In this context, investigation of additional interlayers such as polymer and organic coatings may be a relevant strategy to compensate the fragile behavior of inorganic protective layers.

Declaration of Competing Interests

The authors declare that they have no known competing financial interests or personal relationships that could have appeared to influence the work reported in this paper.

Author statement

Laurent Castro: Investigation, Validation

Emmanuel Petit: Investigation, Validation, Visualization

Anass Benayad: Investigation, Validation, Visualization, Writing - original draft, Writing - review & editing

Fabrice Mauvy: Conceptualization, Methodology, Supervision, Visualization, Writing - original draft, Writing - review & editing

Brigitte Pecquenard: Conceptualization, Methodology, Supervision, Visualization, Writing - original draft, Writing - review & editing

Frédéric Le Cras: Conceptualization, Methodology, Supervision, Visualization, Writing - original draft, Writing - review & editing

Céline Barchasz: Conceptualization, Methodology, Investigation, Validation, Supervision, Visualization, Writing - original draft, Writing - review & editing, Project administration.

Acknowledgements

The authors thank ANR (National Research Agency) PROGELEC program (ANR-12-PRGE-0006-01) for financial support.

References

1. M. Armand, J.-M. Tarascon. Building better batteries. Nature, 451 (2008).
2. T. Placke, R. Kloepsch, S. Dühnen, M. Winter. Lithium ion, lithium metal, and alternative rechargeable battery technologies: the odyssey for high energy density. J. Solid State Electrochem., 21 (2017), pp. 1939-1964.
3. R. Van Noorden. A better battery. Nature, 507 (2014).
4. J.L. Sullivan, L. Gaines. Status of life cycle inventories for batteries. Energy Convers. Manag., 58 (2012), pp. 134-148.
5. J.-M. Tarascon, M. Armand. Issues and challenges facing rechargeable lithium batteries. Nature, 414 (2001).
6. P.G. Bruce, S.A. Freunberger, L.J. Hardwick, J.-M. Tarascon. Li-O2 and Li-S batteries with high energy storage. Nat. Mater., 11 (2012).
7. E.J. Berg, C. Villevieille, D. Streich, S. Trabesinger, P. Novak. Rechargeable batteries: grasping for the limits of chemistry. J. Electrochem. Soc., 162 (2015), pp. A2468-A2475.
8. W. Xu, J. Wang, F. Ding, X. Chen, E. Nasybulin, Y. Zhangad, J.-G. Zhang. Lithium metal anodes for rechargeable batteries. Energy Environ. Sci., 7 (2014), p. 513.

9. M. Hagen, D. Hanselmann, K. Ahlbrecht, R. Maça, D. Gerber, J. Tübke. Lithium–sulfur cells: the gap between the state-of-the-art and the requirements for high energy battery cells. Adv. Energy Mater., 1401986 (2015).
10. Sheng-H. Chung, C.-H. Chang, A. Manthiram. Progress on the critical parameters for lithium–sulfur batteries to be practically viable. Adv. Funct. Mater., 1801188 (2018), pp. 315-338.
11. D. Eroglu, K.R. Zavadil, K.G. Gallagher. Critical link between materials chemistry and cell-level design for high energy density and low cost lithium-sulfur transportation battery. J. Electrochem. Soc., 162 (2015), pp. A982-A990.
12. D. Aurbach, E. Pollak, R. Elazari, G. Salitra, C.S. Kelley, J. Affinito. On the surface chemical aspects of very high energy density, rechargeable Li–sulfur batteries. J. Electrochem. Soc., 156 (2009), pp. A694-A702.
13. F. Wu, J. Qian, R. Chen, J. Lu, L. Li, H. Wu, J. Chen, T. Zhao, Y. Ye, K. Amine. An effective approach to protect lithium anode and improve cycle performance for Li-S batteries. ACS Appl. Mater. Interfaces, 6 (2014), pp. 15542-15549.
14. L. Suo, Y.-S. Hu, H. Li, M. Armand, L. Chen. A new class of solvent-in-salt electrolyte for high-energy rechargeable metallic lithium batteries. Nat. Commun., 4 (2013), p. 1481.
15. C. Barchasz, J.-C. Lepretre, F. Alloin, S. Patoux. Electrochemical properties of ether-based electrolytes for lithium/sulfur rechargeable batteries. J. Electrochem. Soc., 160 (2013), pp. A430-A436.
16. J. Gao, M.A. Lowe, Y. Kiya, H.D. Abruna. Effects of liquid electrolytes on the charge discharge performance of rechargeable lithium/sulfur batteries: electrochemical and in-situ X-ray absorption spectroscopic studies. J. Phys. Chem. C, 115 (2011), pp. 25132-25137.
17. D. Aurbach, E. Granot. The study of electrolyte solutions based on solvents from the "glyme" family (linear polyethers) for secondary Li battery systems. Electrochim. Acta, 42 (1997), pp. 697-718.
18. A. Zaban, E. Zinigrad, D. Aurbach. Impedance spectroscopy of Li electrodes. 4. A general simple model of the Li-solution interphase in polar aprotic systems. J. Phys. Chem., 100 (1996), pp. 3089-3101.
19. D. Aurbach, O. Youngman, Y. Gofer, A. Meitav. The electrochemical behavior of DIOX-LiClO4 solution - I - uncontaminated solutions. Electrochim. Acta, 35 (1990), pp. 625-638.
20. D. Aurbach, O. Youngman, P. Dan. The electrochemical behavior of DIOX-LiClO4 solution - II - contaminated solutions. Electrochim. Acta, 35 (1990), pp. 639-655.
21. Y. Lu, S. Gu, X. Hong, K. Rui, X. Huang, J. Jin, C. Chen, J. Yang, Z. Wen. Pre-modified Li3PS4 based interphase for lithium anode towards high performance Li-S battery. Energy Storage Mater., 11 (2018), pp. 16-23.
22. C. Zu, N. Azimi, Z. Zhang, A. Manthiram. Insight into lithium–metal anodes in lithium–sulfur batteries with a fluorinated ether electrolyte. J. Mater. Chem. A, 3 (2015), p. 14864.
23. M.J. Lacey, A. Yalamanchili, J. Maibach, C. Tengstedt, K. Edström, D. Brandell. The Li–S battery: an investigation of redox shuttle and self-discharge behaviour with LiNO3-containing electrolytes. RSC Adv., 6 (2016), p. 3632.
24. J.-H. Song, J.-T. Yeon, J.-Y. Jang, J.-G. Han, S.-M. Lee, N.-S. Choi. Effect of fluoroethylene carbonate on electrochemical performances of lithium electrodes and lithium-sulfur batteries. J. Electrochem. Soc., 160 (2013), pp. A873-A881.
25. W. Li, H. Yao, K. Yan, G. Zheng, Z. Liang, Y.-M. Chiang, Y. Cui. The synergetic effect of lithium polysulfide and lithium nitrate to prevent lithium dendrite growth. Nat. Commun., 6 (2015), p. 7436.
26. B.D. Adams, E.V. Carino, J.G. Connell, K.S. Han, R. Cao, J. Chen, J. Zheng, Q. Li, K.T. Mueller, W.A. Henderson, J.-G. Zhang. Long term stability of Li-S batteries using high concentration lithium nitrate electrolytes. Nano Energy, 40 (2017), pp. 607-617
27. S. Liatard, K. Benhamouda, A. Fournier, J. Dijon, C. Barchasz. Influence of catholyte composition on the performances of VACNT/Polysulfides/Li cells. Electrochim. Acta, 187 (2016), pp. 670-676.
28. S.-H. Kang, X. Zhao, J. Manuel, H.-J. Ahn, K.-W. Kim, K.-K. Cho, J.-H. Ahn. Effect of sulfur loading on energy density of lithium sulfur batteries. Phys. Status Solidi A, 211 (8) (2014), pp. 1895-1899.
29. B.D. Adams, E.V. Carino, J.G. Connell, K.S. Han, R. Cao, J. Chen, J. Zheng, Q. Li, K.T. Mueller, W.A. Henderson, J.-G. Zhang. Long term stability of Li-S batteries using high concentration lithium nitrate electrolytes. Nano Energy, 40 (2017), pp. 607-617.
30. G. Ma, Z. Wen, M. Wu, C. Shen, Q. Wang, J. Jin, X. Wu. A lithium anode protection guided highly-stable lithium–sulfur battery. Chem. Commun., 50 (2014), p. 14209.
31. L. Chen, J.G. Connell, A. Nie, Z. Huang, K.R. Zavadil, K.C. Klavetter, Y. Yuan, S. Sharifi-Asl, R. Shahbazian-Yassar, J. Libera, A.U. Mane, J.W. Elam. Lithium metal protected by atomic layer deposition metal oxide for high performance anodes. J. Mater. Chem. A, 5 (2017), p. 12297.
32. T. Tao, S. Lu, Y. Fan, W. Lei, S. Huang, Y. Chen. Anode improvement in rechargeable lithium–sulfur batteries. Adv. Mater., 1700542 (2017).
33. G. Zheng, S.W. Lee, Z. Liang, H.-W. Lee, K. Yan, H. Yao, H. Wang, W. Li, S. Chu, Y. Cui. Interconnected hollow carbon nanospheres for stable lithium metal anodes. Nat. Technol., 9 (2014).
34. Y. An, Z. Zhang, H. Fei, X. Xu, S. Xiong, J. Feng, L. Ci. Lithium metal protection enabled by in-situ olefin polymerization for high-performance secondary lithium sulfur batteries. J. Power Sources, 363 (2017), pp. 193-198.
35. Y. Lu, X. Huang, Z. Song, K. Rui, Q. Wang, S. Gu, J. Yang, T. Xiu, M.E. Badding, Z. Wen. Highly stable garnet solid electrolyte based Li-S battery with modified anodic and cathodic interfaces. Energy Storage Mater., 15 (2018), pp. 282-290.

36. C. Sun, X. Huang, J. Jin, Y. Lu, Q. Wang, J. Yang, Z. Wen. An ion-conductive Li1.5Al0.5Ge1.5(PO4)3-based composite protective layer for lithium metal anode in lithium-sulfur batteries. J. Power Sources, 377 (2018), pp. 36-43.
37. A.C. Kozen, C.F. Lin, O. Zhao, S.B. Lee, G.W. Rubloff, M. Noked. Stabilization of lithium metal anodes by hybrid artificial solid electrolyte interphase. Chem. Mater., 29 (2017), pp. 6298-6307.
38. L. Wang, Q. Wang, W. Jia, S. Chen, P. Gao, J. Li. Li metal coated with amorphous Li3PO4 via magnetron sputtering for stable and long-cycle life lithium metal batteries. J. Power Sources, 342 (2017), pp. 175-182.
39. W. Wang, X. Yue, J. Meng, J. Wang, X. Wang, H. Chen, D. Shi, J. Fu, Y. Zhou, J. Chen, Z. Fu. Lithium phosphorus oxynitride as an efficient protective layer on lithium metal anodes for advanced lithium-sulfur batteries. Energy Storage Mater., 18 (2019), pp. 414-422.
40. M. Cretin, PhD thesis, Univ. Grenoble, 1996.
41. B. Fleutot, B. Pecquenard, H. Martinez, M. Letellier, A. Levasseur. Investigation of the local structure of LiPON thin films to better understand the role of nitrogen on their performance. Solid State Ionics, 186 (2011), pp. 29-36.
42. F. Le Cras, B. Pecquenard, V. Dubois, V.-P. Phan, D. Guy-Bouyssou. All-solid-state lithium-ion microbatteries using silicon nanofilm anodes: high performance and memory effect. Adv. Energy Mater., 5 (2015), Article 1501061.
43. B. Fleutot, B. Pecquenard, F. Le Cras, B. Delis, H. Martinez, L. Dupont, D. Guy, Bouyssou. Characterization of all-solid-state Li/LiPONB/TiOS microbatteries produced at the pilot scale. J. Power Sources, 196 (2011), pp. 10289-10296
44. http://www.ohara-inc.co.jp/en/product/electronics/licgcsp01.html
45. K. Kousuke Nakajima, T. Katoh, Y. Inda, B. Hoffman. Lithium ion conductive glass ceramics: properties and application in lithium metal batteries. Symposium on Energy Storage Beyond Lithium Ion; Materials Perspective (2010).
46. E. Lee, T. Kim, A. Benayad, H.-G. Kim, S. Jeon, G.-S. Park. Ar plasma treated ZnON transistor for future thin film electronics. Appl. Phys. Lett., 107 (2015), Article 122105.
47. J.E. Morales-Ugarte, E. Bolimowska, H. Rouault, J. Santos-Peña, C.C. Santini, A. Benayad. EIS and XPS investigation on SEI layer formation during first discharge on graphite electrode with a vinylene carbonate doped imidazolium based ionic liquid electrolyte. J. Phys. Chem. C, 122 (2018), pp. 18223-18230.
48. Q. Wang, J. Jin, X. Wu, G. Ma, J. Yang, Z. Wen. A shuttle effect free lithium sulfur battery based on a hybrid electrolyte. Phys.Chem.Chem.Phys., 16 (2014), p. 21225.